
Article:
Preham, Olivier Yvon Giuseppe, Pinho, Flaviane Alves, Pinto, Ana Isabel orcid.org/0000-0002-9640-6333 et al. (5 more authors) (2018) CD4+ 1 T cells alter the stromal microenvironment and repress medullary erythropoiesis in murine visceral leishmaniasis. Frontiers in immunology. 2958. ISSN 1664-3224

https://doi.org/10.3389/fimmu.2018.02958

$CD4^+$ T cells alter the stromal microenvironment and repress medullary erythropoiesis in murine visceral leishmaniasis.

Olivier Preham[1^], Flaviane A. Pinho[2&], Ana Pinto[1], Gulab Fatima Rani[1], Najmeeyah Brown[1], Ian S. Hitchcock[1], Hiro Goto[2] and Paul M. Kaye[1*]

[1]Centre for Immunology and Infection, Dept of Biology and Hull York Medical School, University of York, Heslington, York, YO10 5DD, UK

[2]Laboratório de Soroepidemiologia e Imunobiologia, Instituto de Medicina Tropical de São Paulo, and Faculdade de Medicina, Universidade de São Paulo, São Paulo, Brazil

^ Current address: UCL Institute of Immunity and Transplantation, Royal Free Hospital, London, NW3 2QG

&Current address: Escola de Medicina Veterinária e Zootecnia, Universidade Federal da Bahia, Salvador, BA, Brazil, 40170-110

Running title: $CD4^+$ T cell repression of erythropoiesis during visceral leishmaniasis.

Keywords: erythropoiesis; stromal cells; macrophages; bone marrow; leishmaniasis.

***Correspondence to**: Prof. Paul M Kaye

paul.kaye@york.ac.uk

Abstract

Human visceral leishmaniasis, a parasitic disease of major public health importance in developing countries, is characterized by variable degrees of severity of anemia, but the mechanisms underlying this change in peripheral blood have not been thoroughly explored. Here, we used an experimental model of visceral leishmaniasis in C57BL/6 mice to explore the basis of anemia following infection with *Leishmania donovani*. 28 days post infection, mice showed bone marrow dyserythropoiesis by myelogram, with a reduction of $TER119^{+}$ $CD71^{-/+}$ erythroblasts. Reduction of medullary erythropoiesis coincided with loss of $CD169^{high}$ bone marrow stromal macrophages and a reduction of CXCL12-expressing stromal cells. Although the spleen is a site of extramedullary erythropoiesis and erythrophagocytosis, splenectomy did not impact the extent of anemia or affect the repression of medullary hematopoiesis that was observed in infected mice. In contrast, these changes in bone marrow erythropoiesis were not evident in B6.*Rag2*$^{-/-}$ mice, but could be fully reconstituted by adoptive transfer of IFNγ-producing but not IFNγ-deficient $CD4^{+}$ T cells, mimicking the expansion of IFNγ-producing $CD4^{+}$ T cells that occurs during infection in wild type mice. Collectively, these data indicate that anemia during experimental murine visceral leishmaniasis can be driven by defects associated with the bone marrow erythropoietic niche, and that this represents a further example of $CD4^{+}$ T cell-mediated immunopathology affecting hematopoietic competence.

Introduction

The bone marrow (BM) is the main site of hematopoiesis in adult mammals and occurs within the cavities of long bones. Hematopoiesis is a complex process through which hematopoietic stem cells (HSCs) proliferate and differentiate into mature blood cells and is largely restricted to specific microenvironments or "niches" that are comprised of a variety of non-hematopoietic stromal cells and secreted factors. The stromal cell-derived chemokine CXCL12 and its receptor CXCR4 are responsible for the retention of HSCs in the BM. Disruption of the CXCL12-CXCR4 axis, or depletion of CXCL12-abundant reticular (CAR) cells, mobilizes HSCs in the peripheral blood [1]. A wide spectrum of diseases impact on hematopoiesis in general and on erythropoiesis in particular by altering these niches, including myeloproliferative neoplasms and infectious diseases [2]. For example, *Escherichia coli* and *Anaplasma phagocytophilum* infections in murine models has been shown to induce CXCL12 down-regulation in the BM and subsequent HSC mobilization [3, 4]. The development of anemia is often complex and multifactorial, as evidenced by experimental studies in infectious disease models and often reflects a balance between erythropoiesis and erythrocyte clearance. For example, in *Trypanosoma brucei* infection, anemia is in part caused by nitric oxide (NO) production, and pro-inflammatory cytokines such as IFNγ and TNF positively correlate with anemia severity [5]. In contrast, direct lysis of RBC is seen during acute malaria [6]. $CD169^+$ BM stromal macrophages are also an essential component of the niche for erythropoiesis [7] as well as important regulators of stromal cells within the HSC niche [8, 9], but less is known about how their function is impacted during infection, or in relation to the development of anemia.

Hematological disturbances are a hallmark of human and canine visceral leishmaniasis (VL) [10, 11], caused by infection with the protozoan parasites *Leishmania donovani* or *L.*

infantum. Differing degrees of cytopenia are associated with disease stage, and as risk factors for VL-related death [12, 13]. VL often results in pancytopenia [14-16] and may sometimes be misdiagnosed as another hematological disorder, such as myelodysplastic syndrome [17]. Various mechanisms have been proposed to underpin the development of VL-associated pancytopenia, including auto-immune destruction of erythrocytes, platelets and leukocytes, or BM failure [18]. Anemia has been attributed to aberrant sialoglycosylation of red blood cells [19], altered recognition of band 3 subsequent to oxidative stress [20] or enhanced macrophage-mediated erythrophagocytosis [21].

While the immune response and hematological consequences of VL have been extensively studied, far less is known about the regulation of hematopoiesis per se during disease, in part due to the ethical challenges involved in studying this in humans. Hematopoiesis has been examined in a hamster model of VL [22], with the finding that *L. donovani* infection induces apoptosis in erythropoietic progenitors in the BM. However, lack of tools for dissecting the hamster immune and hematopoietic microenvironment poses challenges in exploiting this model. Although the mouse model of VL is not lethal, it has been extensively studied to provide more mechanistic data on immunity and immunopathology [23, 24]. However, this model has to date been poorly utilized in the study of hematological dysfunction. Cotterell et al. demonstrated that chronic VL in BALB/c mice results in an increase of hematopoietic progenitors in the spleen and the BM [25], and that BM stromal macrophage-derived cells may become more supportive of myelopoiesis after infection with *L. donovani* in vitro, due to increased secretion of GM-CSF and TNF [26]. More recently, alterations in the HSC compartment have been described that might contribute both to ongoing VL-associated immunosuppression [27] and to long term hematopoietic competence [28].

Here, we have focused on exploring the mechanisms underpinning anemia in C57BL/6 mice infected with *L. donovani.* We show that infected mice develop BM dyserythropoiesis, evidenced both by myelogram and by a reduction of medullar TER119^{+} CD71$^{-/+}$ erythroblasts. Reduction of medullary erythropoiesis coincided with loss of CD169^{high} stromal macrophages and a reduction of CXCL12-expressing stromal cells. We demonstrate, through the use of immunodeficient B6.*Rag2*$^{-/-}$ mice and adoptive cell transfer, that all of these events strictly require the presence of CD4^{+} T cells expressing IFNγ. Hence, we propose that repression of medullary erythropoiesis is added to the catalogue of immunopathological sequelae associated with *Leishmania donovani* infection.

Material and methods

Ethics statement

All animal care and experimental procedures were performed under UK Home Office License (Ref # PPL 60/4377) and with approval from the Animal Welfare and Ethical Review Board of the Department of Biology, University of York.

Mice

C57BL/6, B6.*Rag2*$^{-/-}$, B6.*Cxcl12*$^{tm2.1Sjm/J}$ mice (Jackson Laboratories) and B6.hCD2-DsRed mice were bred at the University of York. IFNγ-KO (B6.129S7-*Ifng*tm1Ts/J, stock no. 002287) mice were obtained from the Jackson Laboratory. All mice were maintained under specific pathogen-free conditions (FELASA 67M standard). As appropriate, mice were micro-chipped, randomly allocated to groups and infected intravenously with 2-3x10^{7} *L. donovani* (LV9) amastigotes isolated from the spleen of infected B6.*Rag2*$^{-/-}$ mice. Mice were splenectomized (Sp$_{x}$) or sham-operated by a commercial supplier (Charles River UK), and

were allowed to recover for 3 weeks before being infected. As required, $6x10^5$ sort-purified splenic $CD45^+CD4^+CD3^+CD8^-B220^-TCR\gamma\delta^-CD49b^-$ cells derived from wild type or IFNγ-KO mice were transplanted into B6.*Rag2*$^{-/-}$.CD45.1Cg recipient mice 24h prior to infection. Unless stated otherwise, experimental mice were killed by cervical dislocation four weeks after infection.

Blood analysis

Blood was collected from terminally anaesthetized mice by cardiac puncture in syringes coated with Citrate-dextrose and transferred into a EDTA-coated Vacutainer®. Blood analysis was performed with a Hemavet 950FS (Drew Scientific)

Bone marrow myelogram

BM samples were obtained by aspiration biopsy from iliac crest using 24 G needle attached to a 5mL disposable plastic syringe with 10% EDTA and smears were stained with May–Grünwald Giemsa (Lewis et al., 2006). Samples were then re-coded for blind analysis. A differential count of 500 cells was made in BM smears to calculate: myeloid : erythroid (M:E) ratio, the myeloid maturation ratio, the erythroid maturation ratio, myeloid precursor cells (myeloblasts + promyelocyte + myelocyte), percentages of myeloid mature cells (metamyelocyte + band neutrophils + segmented neutrophils), erythroid precursor cells ($CD71^+TER119^{lo}$ proerythroblasts + $CD71^{-/+}TER119^{high}$ basophil erythroblasts), erythroid mature cells (polychromatic erythrocyte + orthochromatic erythrocytes; equivalent to $CD71^{-/+}$ $TER119^{high}$), monocytes, macrophages, plasma cells and megakaryocytes according to Yang et al. [40]. The dysplasic features were also analyzed in the myeloid and erythroid series and in megakaryocytes.

Immunohistochemistry

Femurs were isolated and cleaned to remove excessive tissue then fixed overnight at 4°C in periodate-lysine-paraformaldehyde fixative (10mM sodium periodate dissolved in three parts 0.1M lysine-HCl 0.1M Na2HPO4 and one part 20% (w/) paraformaldehyde) and decalcified for 3 days at 4°C with slow agitation in 10% EDTA, 0.1M Tris, pH6.95. Bones were transferred in 30% sucrose in PBS for a final overnight incubation at 4°C. Spleen and bones were embedded in Optimal Cutting Temperature (OCT™) compound (Tissue-Tek) in Cryomolds® (Tissue-Tek) and snap-frozen on dry ice. Spleen and femoral 5µm-sections were cut using a CM1900 cryostat (Leica Microsystems) onto Polysines® slides (Thermo Fisher). Spleen section were fixed in ice-cold acetone for 10min on the day of staining. Sections were blocked in staining buffer (PBS, 0.05% (w/v) BSA, 5% goat serum) for 1h at RT. Excess buffer was removed and slides stained with fluorochrome-labelled TER119, F4/80, CD71 or isotype controls (eBioscience) in staining buffer for 1h at RT or overnight at 4°C. Slides were washes three times for 5min in washing buffer (PBS 0.05% (w/v) BSA) and counterstained with DAPI. Section were mounted in ProLong® Gold antifade reagent (Life Technologies) and sealed before imaging. Confocal images were obtained using LSM780 or LSM710 systems (Leica Microsystems) and analyzed using Zen software (Carl Zeiss). Samples were assessed blind to treatment group.

Flow cytometry

Spleen cells were dissociated using a 70µm cell strainer. Femurs were cut at both ends to expose the bone cavity and the BM was flushed with PBS 1% FCS (flow cytometry buffer) using a 25-gauge needle through a 70µm cell strainer. Single cell suspensions were washed (5min at 300g) and red blood cells were lysed with ACK buffer (5min at RT). Nucleated cells

were subsequently counted using a Vi Cell XR Cell Counter (Beckman Coulter). Cell suspensions were incubated in FcBlock (mouse CD16/32 purified antibody, clone 93) prior to staining with antibodies specific for CD71 (clone R17217), TER119 (clone TER-119), and CD45 (clone 30-F11) or with F4/80 (clone BM8), Ly-6G (clone Gr-1), CD115 (clone AFS98) and CD169 (clone SER-4). For T cell characterization, cells were labeled with in optimized concentration of flurochrome-labelled CD45, CD4 (clone RM4-5 or GK1.5), CD8 (clone 53-7.7), TCRγδ (clone GL-3), B220 (CD45R; clone RA3-6B2)), CD49d (clone DX-5) and CD3 (clone 145-2C11) antibodies diluted in 1x PBS 1% FCS and left at 4°C for 30 min in the dark. Cells were washed and analyzed on a Cyan flow cytometer (Beckman Coulter).

Statistical Analysis

Data were analyzed using GraphPad Prism 5.0 (Prism Software, Irvine, CA, USA). When comparing two groups, Student's t-test or Mann-Whitney test was used according to the data distribution. Welch's correction was applied for the Student's t-test in cases of unequal variances between the two groups. For multiple comparison, one-way ANOVA or Kruskal-Wallis tests were used according to the data distribution followed by Turkey's or Dunn's multiple comparison tests, respectively. Downstream analyses were performed blind to treatment group.

Results

C57BL/6 mice were infected with *L. donovani* amastigotes by the intravenous route and blood parameters were measured over time. Data from naïve mice (n=14) were used to calculate the reference interval, or normal range, for each parameter in the complete blood count. Anemia was first evident at week 4 post infection (**Table 1 and S1 Table**), a time that

193 also represents the approximate peak of infection in spleen and bone marrow [28]. The mean
194 red blood cell (RBC) count per µl of blood was 19% lower in infected mice compared to their
195 naïve counterparts. 70% of infected mice had RBC counts below the normal range. Similarly,
196 the mean hemoglobin (Hb) content in the blood of infected mice was decreased by ~15% in
197 infected mice and ~30% of infected mice had Hb levels below the reference interval. The
198 average volume of erythrocytes was unchanged, with a mean corpuscular volume (MCV) of
199 51 femtoliter (fl) in both groups but 3/13 infected mice (23%) had developed a macrocytic
200 anemia. Although the overall hemoglobin concentration was reduced, all individual mice had
201 mean corpuscular hemoglobin (MCH) values within the normal range. Blood film
202 examination indicated the presence of aberrant red cell morphology with aniso-
203 poikilocytosis, polychromasia, acanthocytes and nucleated red cells (**S1 Fig.**). No significant
204 change in circulating lymphocytes, granulocytes or monocytes was measured between naïve
205 and infected mice, except for a single infected mouse that presented with both lymphopenia
206 and eosinophilia. Thrombocytopenia was evident. These results all point towards
207 development of a normochromic anemia coupled with thrombocytopenia as the most
208 common hematological consequences of *L. donovani* in C57BL/6 mice.
209
210 *Compensatory extra-medullary erythropoiesis occurs in the spleen but medullary*
211 *erythropoiesis is repressed during EVL*
212 Decrease in hematocrit can be caused by reduced numbers of circulating erythrocytes, by
213 impairment of erythropoiesis or by peripheral destruction of RBC. Others have previously
214 reported erythrophagocytosis occurring in the spleen during experimental VL [21], associated
215 with splenomegaly. However, the spleen is also well-known as a site with a propensity for
216 extramedullary hematopoiesis. We confirmed that splenomegaly was associated with extra-
217 medullary erythropoiesis (**Fig. 1**), as determined by an increased frequency (**Fig. 1C and D**)

and absolute number (**Fig. 1E and F**) of $CD45^{-}CD71^{high}TER119^{low}$ pro-erythroblasts and $CD45^{-}CD71^{high/low}TER119^{high}$ erythroblasts [29]. $CD71^{+}TER119^{+}$ cells localized predominantly within the enlarged red pulp (**Fig. 1G**). Hence, during experimental VL, splenomegaly provides both an environment in which splenic clearance of RBCs can occur [21], as well as an environment conducive to enhanced compensatory erythropoiesis.

To determine how anemia and medullary erythropoiesis were altered in the presence or absence of a spleen, we next compared the BM of splenectomized and sham-operated C57BL/6 mice. Decolouration of the femurs was observed in the presence and to a lesser extent in the absence of a spleen **(Fig. 2A)**. Likewise, hematocrit as a measure of anemia was significantly reduced independently of the presence or absence of a spleen **(Fig. 2B)**. We then stained femur sections with TER119. Nucleated $TER119^{+}$ cells were clearly reduced in the BM of infected mice as determined by confocal microscopy **(Fig. 2C and D)**. In contrast to spleen, flow cytometry with CD71 and TER119 indicated that the number of pro-erythroblasts ($CD71^{+}TER119^{low}$ cells) in BM was similar between naïve and infected mice (0.32+/-0.08 vs 0.28+/-0.06) whereas the number of erythroblasts ($CD71^{-/+}TER119^{high}$ cells) in infected mice was significantly reduced compared to the naïve mice (2.66+/- 0.16 vs 0.55+/-0.14; **Fig. 2E and F**). A similar change in erythroblast number was also observed in mice splenectomized prior to infection. Prior to day 28 p.i, we observed no significant alteration in the frequency of BM erythroid precursors (**S2 Fig**). Taken together with the data reported in Pinto et al [28], showing that infection does not affect the absolute number or frequency of myeloid-erythroid progenitors (MEPs) in bone marrow, our data suggest that only the final stages of BM erythropoiesis are impaired in *L. donovani*-infected mice, and that this occurs independently of splenomegaly and splenic function.

Myelogram of BM

To further characterize changes in cellularity of the BM, myeloid and erythroid cells were analyzed by differential counting **(Table 2)**. Infected mice had an increased myeloid: erythroid ratio. Notably, infected mice had an increase in the index of myeloid maturation compared to naive mice, characterized by a high frequency of immature myeloid cells with a decrease in mature myeloid cells. A significant reduction of enucleated mature erythroid cells was also observed, suggesting disturbance in the maturation process and consistent with the anemia observed in blood. In contrast, the frequency of lymphocytes and macrophages was elevated. By morphology, alterations suggestive of dysplasia in the myeloid and erythroid series, including maturation asynchrony (nuclei : cytoplasm asynchrony), giant band cell, megalocyte, fragmented nuclei, binucleated cells and/or bilobed nuclei and atypical mitosis were all observed in infected mice. Other findings included emperipolesis and leuco-erythrophagocytosis **(S3 Fig.)**

The bone marrow microenvironment is altered during EVL

To focus more specifically on cellular changes associated with erythropoiesis, we next examined two major components of the erythropoietic niche, stromal macrophages and CXCL12-abundant reticular (CAR) cells. $CD169^+$ BM stromal macrophages have been reported by others to be important for supporting the later stages of erythropoiesis[7] and are identified as Gr-1^- $CD115^-$ $F4/80^+$ low side scatter (SSC^{low}) cells [7] with surface expression of CD169 (**Fig. 3A and B**). In naïve mice, $CD169^{low}$ and $CD169^{high}$ stromal macrophages could be clearly resolved (**Fig. 3B**). Although the total number of Gr-1^- $CD115^-$ $F4/80^+$ SSC^{low} macrophages was similar between infected and naïve mice **(Fig. 3C)**, the ratio of $CD169^{low}$: $CD169^{high}$ populations was significantly altered. In naive mice, $CD169^{low}$ macrophages accounted for 2.77±0.59% of bone marrow cells or ~$5.x10^5$ cells per

268 femur/tibia, whereas CD169^{high} stromal macrophages accounted for 1.70±0.29% of total bone
269 marrow cells (~3.5x10^5 per femur/tibia). In contrast, in infected mice a clear population of
270 CD169^{high} stromal cells was not apparent (**Fig. 3B**), and numbers of cells gated as positive for
271 CD169 expression was reduced to 2.14x10^5 per femur/tibia (**Fig. 3C**). These data suggest
272 that either there is a loss of CD169 expression by BM stromal macrophages as a consequence
273 of the environment created by infection, or that these cells are lost and replaced in equivalent
274 numbers by other macrophages that lack CD169. The latter is consistent with the evidence
275 provided above of enhanced BM myelopoiesis (**Table 2**).
276
277 CD169$^+$ stromal macrophages are known to interact with stromal reticular cells that produce
278 CXCL12 (CAR cells) and that these are composed of mesenchymal stem and progenitor cells
279 MSPCs [30]. Therefore, we examined expression of CXCL12 at both protein and mRNA
280 levels. RT-qPCR analysis of total BM cells from chronically infected C57BL/6 mice
281 indicated a 50% reduction in *Cxcl12* mRNA accumulation compared to naïve mice **(Fig. 4A)**.
282 We next used CXCL12 reporter mice to identify and quantitate CAR cells expressing this
283 chemokine. By confocal microscopy, there was a clear reduction in the frequency of cells
284 expressing CXCL12 in infected compared to naïve mice (**Fig. 4B**). As the extensive
285 ramifications of these cells made quantification difficult, we performed flow cytometry to
286 validate these data (**Fig. 4C and D**). In naïve B6.*Cxcl12*^{DsRed} mice, the frequency of CAR
287 cells was 0.32±0.02% of total bone marrow cells, corresponding to 4.84±0.49x10^4 cells per
288 femur/tibia. In contrast, the frequency and absolute number of Ds-Red$^+$ cells were reduced in
289 infected mice (0.11±0.01% and 1.36±0.20x10^4 cells per femur) **(Fig. 4E and F)**. Finally, to
290 provide a functional confirmation of reduced numbers of CAR cells, we made use of the
291 property of these cells to generate adherent fibroblastic colonies (CFU-F) *in vitro* [31]. We
292 found a reduction in the absolute number of CFU-F in the BM of infected mice (from

293 32.6±3.4 CFU-F / 1x10^6 BM cells to 11.8±4.5 CFU-F / 1x10^6 BM cells in naïve and infected
294 mice, respectively; **Fig. 4G**). Taken together, these results suggest that mice infected with *L.*
295 *donovani* have reduced levels of stromal cell support for late-stage erythropoiesis in the BM.
296
297 *Bone marrow failure is linked to the adaptive immune response*
298 In addition to being a site of hematopoiesis, the BM is also a site of *L. donovani* infection
299 [25, 28]. To determine whether cell mediated immunity impacted on medullary
300 erythropoiesis, we first assessed the number of lymphocytes in the BM of infected mice. As
301 previously described [28], both $CD4^+$ and $CD8^+$ T cells were found to accumulate in the BM
302 of infected mice, though an expansion in the frequency of $CD4^+$ T cells represented the major
303 change observed (**Fig. 5A** and **S4 Figure**). Accumulation of T cells was also confirmed by
304 confocal microscopy of femur sections in B6.hCD2-GFP mice (**Fig. 5B**). In contrast, we
305 observed no change in the frequency of $CD1b^+$ cells and a compensatory decrease in the
306 frequency of B cells. Of note, similar changes were also observed in mice which had
307 undergone splenectomy prior to infection, indicating that the spleen plays a limited role in the
308 accumulation of bone marrow-homing T cells during infection (**Fig. 5A**).
309
310 We next examined erythropoiesis in the BM of B6.*Rag2*$^{-/-}$ mice by flow cytometry to
311 determine whether adaptive immunity played a role in the suppression of medullary
312 erythropoiesis. As in wild type mice, B6.*Rag2*$^{-/-}$ mice infected with *L. donovani* had similar
313 numbers of pro-erythroblasts as control uninfected mice (**Fig. 5C**), despite significantly
314 higher systemic parasite burden (**S5 Fig**.). In contrast, whereas wild type mice had
315 significantly reduced numbers of erythroblasts, only a modest and not significant reduction in
316 these cells was observed in infected B6.*Rag2*$^{-/-}$ mice **(Fig. 5D)**. Similarly, B6.*Rag2*$^{-/-}$ mice
317 showed no reduction of *Cxcl12* mRNA accumulation after 4 weeks of infection compared to

318 the ~50% reduction seen in wild-type mice **(Fig. 5E)**. In addition, there was no change in the
319 expression of CD169^{high} on Gr-1^{-} CD115^{-} F4/80^{+} SSC^{low} bone marrow macrophages **(Fig.**
320 **5F)**, and the ratio of CD169^{low} and CD169^{high} bone marrow stromal macrophages was similar
321 between the infected and naïve RAG2$^{-/-}$ mice **(Fig. 5G)**.
322
323 Finally, we reconstituted B6.*Rag2*$^{-/-}$ mice by adoptive transfer of CD4^{+} T cells prior to
324 infection with *L. donovani.* B6.*Rag2*$^{-/-}$ mice receiving CD4^{+} T cells displayed anemia similar
325 to wild type immunocompetent mice, as measured by both erythrocyte count and hematocrit
326 (**Fig. 5H and I**) . In contrast to these results obtained using adoptively transferred wild type
327 CD4^{+} T cells, CD4^{+} T cells isolated from IFNγ-deficient B6.*Ifnγ*$^{-/-}$ mice we unable to induce
328 anemia (**Fig. 5H and I**), despite equally efficient engraftment and activation (**S6 Figure**).
329 As expected, IFNγ KO T cells were defective compared to wild type CD4^{+} T cells in terms of
330 controlling systemic parasite load (**S7 Figure**). Collectively, these data support the
331 conclusion that both the medullary changes in erythropoiesis and peripheral anemia seen in
332 experimental VL arise as a consequence of CD4^{+} T cell activation and IFNγ production,
333 independently of any potential contributions from splenomegaly.
334
335
336 **Discussion**
337 Although evidence abounds that VL causes hematological alterations in humans, dogs and
338 experimental model such as hamsters, very little is known about the underlying mechanisms.
339 In the present study, we show using an experimental murine model that CD4^{+} T cell-
340 dependent adaptive immune responses to *L. donovani* underpin anemia through a pathway
341 that involves repressed BM erythropoiesis consequent on alterations in the stromal
342 microenvironment of the erythropoietic niche.

We show here that C57BL/6 mice chronically infected with *L. donovani* presented with a bi-cytopenia characterized by normocytic anemia and thrombocytopenia. These findings are consistent with the hematological data typically reported in human studies of VL, though indicate that in this strain of mice at least, there is no accompanying leucopenia. Anemia is often complex and multifactorial and it is likely that different models of disease may to a greater or lesser extent exemplify different underlying mechanisms. For example, multiple mechanisms have been proposed based on clinical observations for the profound anemia observed in human VL, including immune-mediated hemolysis [32] or splenic sequestration [10, 32, 33]. In hamsters infected with *L. donovani*, anemia associated with lethal infection was correlated with increased apoptosis of erythroid progenitors and an increase of IFNγ in the BM and spleen [21]. Our data in murine VL indicates that the spleen may have counteracting roles, on the one hand permitting enhanced erythrophagocytosis [21], but on the other serving as a site of extramedullary compensatory erythropoiesis. Indeed, it is likely that these events may balance each other, resulting in a mild anemia in intact mice that is subsequently unaltered by splenectomy. The fact that a mild anemia is present in infected mice independent of the presence or absence of a spleen, with dysplastic erythroid features, provides a convenient tool to allow exploration of pathological mechanisms operating within the BM microenvironment. Although we also observe thrombocytopenia in *L. donovani*-infected mice, the mechanisms regulating this process appear distinct from that controlling erythropoiesis and will be reported elsewhere.

Our analysis of the BM microenvironment that supports erythropoiesis has for the first time demonstrated that anemia in murine models of VL represents an aspect of $CD4^+$ T cell mediated immunopathology. BM resident stromal macrophages, identified by the expression

368 of the sialoadhesin CD169 [34], were reduced in number in infected mice. $CD169^+$ stromal
369 macrophages have been shown to be essential for stress erythropoiesis e.g. following
370 chemically-induced anemia, but their depletion causes minimal disruption of physiological
371 erythropoiesis. In these studies, there was no correlation between overt anemia and a
372 reduction of erythroid progenitors in the BM [7]. These data are in line with our
373 observations, since in our model of EVL, chronic infection results only in a mild anemia
374 despite a dramatic reduction of erythroid progenitors in the bone marrow as observed in
375 myelogram and flow cytometry analysis. We have previously shown that *L.donovani*
376 amastigotes readily parasitize $CD169^+$ BM stromal macrophages during chronic infection and
377 that infection of these cells directly supports an increase in their capacity to support
378 myelopoiesis [26]. Our current data extends these observations by indicating that the
379 reduction of the number of $CD169^+$ stromal macrophages is not a direct consequence of
380 parasitism, as infected B6.*Rag2*$^{-/-}$ mice have significantly increased parasite loads in the BM,
381 yet show no changes in stromal macrophage number. Rather, our data suggest that loss of
382 stromal macrophages is a further consequence of T cell dependent immune responses.
383
384 While $CD169^+$ stromal macrophages were reduced in number, the total number of BM
385 macrophages remained stable or increased during infection. It is unclear if loss of $CD169^+$
386 stromal macrophages represents depletion or conversion to a different phenotype, for which
387 specific lineage tracking studies would be required. STING-mediated activation of BM
388 $CD169^+$ macrophages has been shown to be essential to type I IFN production by
389 plasmacytoid dendritic in a malaria mouse model [35], indicating that these cells are directly
390 sensitive to infections. Similarly, dexamethasone treatment induces CD169 expression on the
391 surface of human macrophages, promoting in the same time their erythropoiesis-supporting
392 function [36]. Hence, the a stromal "CD169" phenotype can be acquired in differentiated

393 macrophages and is responsive to inflammatory signals. Interestingly, dexamethasone is also
394 an inhibitor of iNOS [37], thus suggesting a role for NO in EVL-induced anemia.
395 Previously, $CD169^+$ macrophages have been shown to be depleted by G-CSF administration
396 [38]. We have observed a consistent upregulation of circulating G-CSF in infected mice (data
397 not shown) but to date our attempts to convincingly neutralize G-CSF in vivo have been
398 unsuccessful. Hence, direct evidence is still needed to support a role for G-CSF in VL-
399 induced anemia.
400
401 In hamsters and mice, infection with *L. donovani* causes an increase of erythroid burst
402 forming units (BFU-E) from the bone marrow in colony formation assays [22, 25]. These
403 represent very early progenitors of erythroid cells, prior to the pro-erythroblast stage. In the
404 current study, we show by flow cytometry that only later stages of erythroid differentiation,
405 at or after the pro-erythroblast stage, are affected by infection. This is also reflected in
406 differential counts of bone marrow cells, showing that nucleated mature erythroid cells were
407 reduced in infected mice. Furthermore, conditional depletion of $CD169^+$ cells in a mouse
408 model did not alter the BFU-E content in the BM of mice [7]. These data are collectively
409 consistent with macrophage-dependent erythroblastic islands functioning to support
410 erythropoiesis from the erythroblast stage onwards.
411
412 We also report that CXCL12-producing mesenchymal stromal cells are affected during VL.
413 Infection led to a reduction of *Cxcl12* mRNA accumulation in the bone marrow, correlating
414 with a reduction in the number of CXCL12-expressing cells. The main mechanism of G-
415 CSF-induced down-regulation of CXCL12 is protease-dependent [39] but a more complex
416 model including transcriptional regulation has also been reported. While down-regulation of
417 CXCL12 is a potentially due to up-regulation of G-CSF, CD169 macrophages are also

418 responsible for the retention of CAR cells in the bone marrow. It is likely that these
419 mechanisms together factor into the loss of stromal support in the BM. In the case of *E coli.*
420 infection, heightened levels of G-CSF led to a reduction in CXCL12 expression in the BM
421 via Toll-like receptor and NOD1/2 signaling [3]. This study did not however directly
422 enumerate CXCL12-producing cells in BM, our observations here being the first reported
423 instance of loss of these cells during infectious disease.
424
425 In summary, we have shown that IFNγ-producing $CD4^+$ T cells contribute to anemia in a
426 model of VL, via a mechanism that involves loss of both macrophages and mesenchymal
427 stromal elements from the BM erythropoietic niche leading to dyserythropoiesis. Whether
428 these effects are the result of direct IFNγ signaling on $CD169^+$ macrophages and / or
429 mesenchymal stromal cells, whether they reflect indirect effects of IFNγ on third party cells
430 or whether they are the consequence of induced expression of one of the many IFN-
431 responsive genes remains to be determined. We have also recently shown that $CD4^+$ T cells
432 producing both IFNγ and TNF accumulate in large numbers in the BM of infected mice, via a
433 mechanism requiring $CD4^+$ T cell-intrinsic TNF receptor signaling. These cells drive
434 functional exhaustion within the long-term HSC compartment [28]. Collectively, therefore,
435 a picture emerges whereby $CD4^+$ T cells play a pathogenic role in the BM that leads to BM
436 failure with both short and long-term consequences for hematological health. These data
437 provide an imperative for similar studies in humans, to determine whether $CD4^+$ T cells
438 likewise have a causative role in the hematological changes associated with VL or indeed
439 other infections where BM accumulation of activated effector T cells occurs.
440
441
442 **Acknowledgements**

443 The authors thank the staff of the Biological Services Facility for animal husbandry and the
444 staff of the BioSciences Technology Facility Imaging and Cytometry Laboratory for
445 assistance with flow and confocal analysis.

References

1. Sugiyama T, Kohara H, Noda M, Nagasawa T. Maintenance of the hematopoietic stem cell pool by CXCL12-CXCR4 chemokine signaling in bone marrow stromal cell niches. Immunity. 2006;25(6):977-88. Epub 2006/12/19. doi: 10.1016/j.immuni.2006.10.016. PubMed PMID: 17174120.

2. Pietras EM. Inflammation: a key regulator of hematopoietic stem cell fate in health and disease. Blood. 2017;130(15):1693-8. Epub 2017/09/07. doi: 10.1182/blood-2017-06-780882. PubMed PMID: 28874349; PubMed Central PMCID: PMCPMC5639485.

3. Burberry A, Zeng MY, Ding L, Wicks I, Inohara N, Morrison SJ, et al. Infection mobilizes hematopoietic stem cells through cooperative NOD-like receptor and Toll-like receptor signaling. Cell Host Microbe. 2014;15(6):779-91. Epub 2014/06/03. doi: 10.1016/j.chom.2014.05.004. PubMed PMID: 24882704; PubMed Central PMCID: PMCPMC4085166.

4. Johns JL, Borjesson DL. Downregulation of CXCL12 signaling and altered hematopoietic stem and progenitor cell trafficking in a murine model of acute Anaplasma phagocytophilum infection. Innate Immun. 2012;18(3):418-28. Epub 2011/10/04. doi: 10.1177/1753425911413794. PubMed PMID: 21964802; PubMed Central PMCID: PMCPMC3905609.

5. Musaya J, Matovu E, Nyirenda M, Chisi J. Role of cytokines in Trypanosoma brucei-induced anaemia: A review of the literature. Malawi Med J. 2015;27(2):45-50. Epub 2015/09/26. PubMed PMID: 26405511; PubMed Central PMCID: PMCPMC4562079.

6. Ghosh K, Ghosh K. Pathogenesis of anemia in malaria: a concise review. Parasitol Res. 2007;101(6):1463-9. Epub 2007/09/18. doi: 10.1007/s00436-007-0742-1. PubMed PMID: 17874326.

7. Chow A, Huggins M, Ahmed J, Hashimoto D, Lucas D, Kunisaki Y, et al. CD169(+) macrophages provide a niche promoting erythropoiesis under homeostasis and stress. Nat Med. 2013;19(4):429-36. Epub 2013/03/19. doi: 10.1038/nm.3057. PubMed PMID: 23502962; PubMed Central PMCID: PMCPMC3983996.

8. Casanova-Acebes M, Pitaval C, Weiss LA, Nombela-Arrieta C, Chevre R, N AG, et al. Rhythmic modulation of the hematopoietic niche through neutrophil clearance. Cell. 2013;153(5):1025-35. Epub 2013/05/28. doi: 10.1016/j.cell.2013.04.040. PubMed PMID: 23706740; PubMed Central PMCID: PMCPMC4128329.

9. Chow A, Lucas D, Hidalgo A, Mendez-Ferrer S, Hashimoto D, Scheiermann C, et al. Bone marrow CD169+ macrophages promote the retention of hematopoietic stem and progenitor cells in the mesenchymal stem cell niche. J Exp Med. 2011;208(2):261-71. Epub 2011/02/02. doi: 10.1084/jem.20101688. PubMed PMID: 21282381; PubMed Central PMCID: PMCPMC3039855.

10. Cartwright GE, Chung HL, Chang A. Studies on the pancytopenia of kala-azar. Blood. 1948;3(3):249-75. Epub 1948/03/01. PubMed PMID: 18902574.

11. Goto Y, Cheng J, Omachi S, Morimoto A. Prevalence, severity, and pathogeneses of anemia in visceral leishmaniasis. Parasitol Res. 2017;116(2):457-64. Epub 2016/11/09. doi: 10.1007/s00436-016-5313-x. PubMed PMID: 27822583.

12. Belo VS, Struchiner CJ, Barbosa DS, Nascimento BW, Horta MA, da Silva ES, et al. Risk factors for adverse prognosis and death in American visceral leishmaniasis: a meta-

490 analysis. PLoS Negl Trop Dis. 2014;8(7):e2982. Epub 2014/07/25. doi:
491 10.1371/journal.pntd.0002982. PubMed PMID: 25058582; PubMed Central PMCID:
492 PMCPMC4109848.

493 13. Coura-Vital W, Araujo VE, Reis IA, Amancio FF, Reis AB, Carneiro M. Prognostic
494 factors and scoring system for death from visceral leishmaniasis: an historical cohort study in
495 Brazil. PLoS Negl Trop Dis. 2014;8(12):e3374. Epub 2014/12/17. doi:
496 10.1371/journal.pntd.0003374. PubMed PMID: 25503575; PubMed Central PMCID:
497 PMCPMC4263605.

498 14. Alexandropoulou O, Tsolia M, Kossiva L, Giannaki M, Karavanaki K. Visceral
499 leishmaniasis: a common cause of post-infectious febrile pancytopenia in children in an
500 endemic area: experience of a children's tertiary hospital. Pediatr Emerg Care.
501 2012;28(6):533-7. Epub 2012/06/02. doi: 10.1097/PEC.0b013e3182587d5d. PubMed PMID:
502 22653455.

503 15. Besada E, Njalla RJ, Nossent JC. Imported case of visceral leishmaniasis presenting
504 as pancytopenia in a Norwegian patient treated with methotrexate and etanercept for psoriasis
505 arthritis. Rheumatol Int. 2013;33(10):2687-9. Epub 2012/08/14. doi: 10.1007/s00296-012-
506 2483-4. PubMed PMID: 22886470.

507 16. Koster KL, Laws HJ, Troeger A, Meisel R, Borkhardt A, Oommen PT. Visceral
508 Leishmaniasis as a Possible Reason for Pancytopenia. Front Pediatr. 2015;3:59. Epub
509 2015/07/16. doi: 10.3389/fped.2015.00059. PubMed PMID: 26176005; PubMed Central
510 PMCID: PMCPMC4483513.

511 17. Kopterides P, Halikias S, Tsavaris N. Visceral leishmaniasis masquerading as
512 myelodysplasia. Am J Hematol. 2003;74(3):198-9. Epub 2003/10/31. doi: 10.1002/ajh.10408.
513 PubMed PMID: 14587050.

514 18. Yarali N, Fisgin T, Duru F, Kara A. Myelodysplastic features in visceral
515 leishmaniasis. Am J Hematol. 2002;71(3):191-5. Epub 2002/11/01. doi: 10.1002/ajh.10200.
516 PubMed PMID: 12410574.

517 19. Samanta S, Ghoshal A, Bhattacharya K, Saha B, Walden P, Mandal C.
518 Sialoglycosylation of RBC in visceral leishmaniasis leads to enhanced oxidative stress,
519 calpain-induced fragmentation of spectrin and hemolysis. PLoS One. 2012;7(7):e42361.
520 Epub 2012/08/04. doi: 10.1371/journal.pone.0042361. PubMed PMID: 22860118; PubMed
521 Central PMCID: PMCPMC3409180.

522 20. Saha Roy S, Chowdhury KD, Sen G, Biswas T. Oxidation of hemoglobin and
523 redistribution of band 3 promote erythrophagocytosis in visceral leishmaniasis. Mol Cell
524 Biochem. 2009;321(1-2):53-63. Epub 2008/09/09. doi: 10.1007/s11010-008-9909-z. PubMed
525 PMID: 18777164.

526 21. Morimoto A, Omachi S, Osada Y, Chambers JK, Uchida K, Sanjoba C, et al.
527 Hemophagocytosis in Experimental Visceral Leishmaniasis by Leishmania donovani. PLoS
528 Negl Trop Dis. 2016;10(3):e0004505. Epub 2016/03/05. doi: 10.1371/journal.pntd.0004505.
529 PubMed PMID: 26942577; PubMed Central PMCID: PMCPMC4778860.

530 22. Lafuse WP, Story R, Mahylis J, Gupta G, Varikuti S, Steinkamp H, et al. Leishmania
531 donovani infection induces anemia in hamsters by differentially altering erythropoiesis in
532 bone marrow and spleen. PLoS One. 2013;8(3):e59509. Epub 2013/03/28. doi:
533 10.1371/journal.pone.0059509. PubMed PMID: 23533629; PubMed Central PMCID:
534 PMCPMC3606219.

23. Bankoti R, Stager S. Differential Regulation of the Immune Response in the Spleen and Liver of Mice Infected with Leishmania donovani. J Trop Med. 2012;2012:639304. Epub 2011/08/04. doi: 10.1155/2012/639304. PubMed PMID: 21811511; PubMed Central PMCID: PMCPMC3143424.

24. Engwerda CR, Ato M, Kaye PM. Macrophages, pathology and parasite persistence in experimental visceral leishmaniasis. Trends Parasitol. 2004;20(11):524-30. Epub 2004/10/09. doi: 10.1016/j.pt.2004.08.009. PubMed PMID: 15471704.

25. Cotterell SE, Engwerda CR, Kaye PM. Enhanced hematopoietic activity accompanies parasite expansion in the spleen and bone marrow of mice infected with Leishmania donovani. Infect Immun. 2000;68(4):1840-8. Epub 2000/03/18. PubMed PMID: 10722572; PubMed Central PMCID: PMCPMC97356.

26. Cotterell SE, Engwerda CR, Kaye PM. Leishmania donovani infection of bone marrow stromal macrophages selectively enhances myelopoiesis, by a mechanism involving GM-CSF and TNF-alpha. Blood. 2000;95(5):1642-51. Epub 2000/02/26. PubMed PMID: 10688819.

27. Abidin BM, Hammami A, Stager S, Heinonen KM. Infection-adapted emergency hematopoiesis promotes visceral leishmaniasis. PLoS Pathog. 2017;13(8):e1006422. Epub 2017/08/09. doi: 10.1371/journal.ppat.1006422. PubMed PMID: 28787450; PubMed Central PMCID: PMCPMC5560750.

28. Pinto AI, Brown N, Preham O, Doehl JSP, Ashwin H, Kaye PM. TNF signalling drives expansion of bone marrow CD4+ T cells responsible for HSC exhaustion in experimental visceral leishmaniasis. PLoS Pathog. 2017;13(7):e1006465. Epub 2017/07/04. doi: 10.1371/journal.ppat.1006465. PubMed PMID: 28671989; PubMed Central PMCID: PMCPMC5510901.

29. Koulnis M, Pop R, Porpiglia E, Shearstone JR, Hidalgo D, Socolovsky M. Identification and analysis of mouse erythroid progenitors using the CD71/TER119 flow-cytometric assay. J Vis Exp. 2011;(54). Epub 2011/08/19. doi: 10.3791/2809. PubMed PMID: 21847081; PubMed Central PMCID: PMCPMC3211121.

30. Omatsu Y, Sugiyama T, Kohara H, Kondoh G, Fujii N, Kohno K, et al. The essential functions of adipo-osteogenic progenitors as the hematopoietic stem and progenitor cell niche. Immunity. 2010;33(3):387-99. Epub 2010/09/21. doi: 10.1016/j.immuni.2010.08.017. PubMed PMID: 20850355.

31. Frenette PS, Pinho S, Lucas D, Scheiermann C. Mesenchymal stem cell: keystone of the hematopoietic stem cell niche and a stepping-stone for regenerative medicine. Annu Rev Immunol. 2013;31:285-316. Epub 2013/01/10. doi: 10.1146/annurev-immunol-032712-095919. PubMed PMID: 23298209.

32. Woodruff AW, Topley E, Knight R, Downie CG. The anaemia of kala-azar. Br J Haematol. 1972;22(3):319-29. Epub 1972/03/01. PubMed PMID: 4552217.

33. Varma N, Naseem S. Hematologic changes in visceral leishmaniasis/kala azar. Indian J Hematol Blood Transfus. 2010;26(3):78-82. Epub 2011/09/03. doi: 10.1007/s12288-010-0027-1. PubMed PMID: 21886387; PubMed Central PMCID: PMCPMC3002089.

34. Crocker PR, Gordon S. Mouse macrophage hemagglutinin (sheep erythrocyte receptor) with specificity for sialylated glycoconjugates characterized by a monoclonal antibody. J Exp Med. 1989;169(4):1333-46. Epub 1989/04/01. PubMed PMID: 2926328; PubMed Central PMCID: PMCPMC2189241.

35. Spaulding E, Fooksman D, Moore JM, Saidi A, Feintuch CM, Reizis B, et al. STING-Licensed Macrophages Prime Type I IFN Production by Plasmacytoid Dendritic Cells in the Bone Marrow during Severe Plasmodium yoelii Malaria. PLoS Pathog. 2016;12(10):e1005975. Epub 2016/10/30. doi: 10.1371/journal.ppat.1005975. PubMed PMID: 27792766; PubMed Central PMCID: PMCPMC5085251.

36. Heideveld E, Hampton-O'Neil LA, Cross SJ, van Alphen FPJ, van den Biggelaar M, Toye AM, et al. Glucocorticoids induce differentiation of monocytes towards macrophages that share functional and phenotypical aspects with erythroblastic island macrophages. Haematologica. 2017. Epub 2017/12/30. doi: 10.3324/haematol.2017.179341. PubMed PMID: 29284682.

37. Soderberg M, Raffalli-Mathieu F, Lang MA. Regulation of the murine inducible nitric oxide synthase gene by dexamethasone involves a heterogeneous nuclear ribonucleoprotein I (hnRNPI) dependent pathway. Mol Immunol. 2007;44(12):3204-10. Epub 2007/03/24. doi: 10.1016/j.molimm.2007.01.029. PubMed PMID: 17379310.

38. Jacobsen RN, Forristal CE, Raggatt LJ, Nowlan B, Barbier V, Kaur S, et al. Mobilization with granulocyte colony-stimulating factor blocks medullar erythropoiesis by depleting F4/80(+)VCAM1(+)CD169(+)ER-HR3(+)Ly6G(+) erythroid island macrophages in the mouse. Exp Hematol. 2014;42(7):547-61 e4. Epub 2014/04/12. doi: 10.1016/j.exphem.2014.03.009. PubMed PMID: 24721610.

39. Levesque JP, Liu F, Simmons PJ, Betsuyaku T, Senior RM, Pham C, et al. Characterization of hematopoietic progenitor mobilization in protease-deficient mice. Blood. 2004;104(1):65-72. Epub 2004/03/11. doi: 10.1182/blood-2003-05-1589. PubMed PMID: 15010367.

40. Yang M, Busche G, Ganser A, Li Z. Morphology and quantitative composition of hematopoietic cells in murine bone marrow and spleen of healthy subjects. Ann Hematol. 2013;92(5):587-94. Epub 2013/01/12. doi: 10.1007/s00277-012-1653-5. PubMed PMID: 23307597.

610 **Figure Legends.**

611

612 **Fig. 1. *L. donovani* infection induces extramedullary erythropoiesis in the spleen.**

613 **A and B**. Gating strategy for identification of pro-erythroblasts ($CD45^-CD71^{high}TER119^{low}$) and

614 erythroblasts ($CD45^-CD71^{high/low}TER119^{high}$) in the spleens of naïve (A) and infected (B) mice.

615 Plots are gated on $CD45^-$ live cells and equal number of live cells. **C**. Frequency of pro-

616 erythroblasts in the spleen. **D.** Frequency of erythroblasts in the spleen. **E**. Absolute number of

617 pro-erythroblasts per spleen. **F.** Absolute number of erythroblasts per spleen. Absolute numbers

618 were calculated by multiplying the cell frequencies by the total numbers of cells per spleen. **G**

619 **and H**. Representative histology of spleens from control (G) and infected (H) mice. Sections

620 were stained for F4/80 (green), TER119 (white) CD71 (red) and counterstained with DAPI

621 (Blue). F4/80 demarcates the red pulp. All mice were infected for 28 days. Data represent mean

622 ± SEM (unpaired t-test with Welch's correction; n=8 mice per group from two independent

623 experiments).

624

625 **Fig. 2. Medullary erythropoiesis is repressed during experimental visceral leishmaniasis**

626 **A.** Femurs isolated from *L. donovani*-infected mice and age-matched naïve mice. Representative

627 from 30 mice per group from 10 independent experiment. **B.** Hematocrit in naïve and infected

628 mice with and without splenectomy (Sp_x). **C and D**. Confocal imaging of 5µm-thick femoral

629 sections from naïve (C) and infected (D) mice stained with DAPI (blue) and TER119 (white).

630 Representative of 6 mice per group from 2 independent experiments. **E.** Representative flow

631 cytometry analysis of $CD45^-$ BM cells from infected mouse using the erythroid surface markers

632 CD71 (transferrin receptor) and TER-119. Pro-erythroblasts are $CD45^-CD71^+TER119^{low}$ and

633 erythroblasts are $CD45^-CD71^{-/+}TER119^{high}$. **F.** Absolute number of pro-erythroblasts per femur

634 + tibia in sham operated and Sp_x mice. Mann Whitney test; n=14 mice per group from 4

independent experiments. Data represent mean ± SEM. All experiments were performed 28 days post-infection.

Fig. 3. Infection with *L. donovani* reduces the number of CD169^{+} stromal macrophages in BM.

A. BM stromal macrophages were identified as Gr-1^{-} CD115^{-} F4/80^{+} SSC^{low} cells [9]. **B.** CD169 expression on BM macrophages of naïve (green) and infected (red) mice. Isotype control (blue) is representative of both naïve and infected mice. **C.** Absolute number of macrophages per leg (1 femur + 1 tibia) according to the gating described in A and B. **D.** Absolute number of CD169^{low} and CD169^{high} stromal macrophages based on gating in B. Absolute numbers were calculated from the frequencies multiplied by the total bone marrow cells isolated from each mouse. Data represent mean ± SEM. All experiments were performed 28 days after infection. (unpaired t-test; n=10 mice per group from 2 independent experiments)

Fig. 4. *L. donovani* infection causes a reduction in CXCL-12-expressing cells in the BM.

A. *Cxcl12* mRNA accumulation in BM of naïve and infected mice, determined by qRT-PCR. **B**. Visualisation of CXCL12-expressing cells using naïve and infected *Cxcl12*-DsRed reporter mice. Sectioned were co-stained for laminin (green) and counterstained with DAPI (blue). **C and D.** Flow cytometry analysis of DsRed^{+} cells in naïve (C) and infected (D) *Cxcl12*-DsRed reporter mice. Dot plots show identical number of cells, gated on live single cells. **E.** Frequency of DsRed^{+} cells. **F.** Absolute number of DsRed^{+} cells per femur, calculated from the frequency of DsRed^{+} cells in (E) multiplied by the total bone marrow cell count (Mann Whitney test; Data from 5 naïve mice and 9 infected mice from 2 independent experiments). **G.** Number of CFU-F per million BM cells (Unpaired t-test; n=7 mice per group from 2 independent experiments). Data represent mean ± SEM. All experiments were performed 28 days post-infection with *L. donovani*.

Fig. 5 IFNγ-producing CD4$^+$ T cells mediate repression of medullary erythropoiesis in experimental VL.

A. Frequency of leucocyte subsets accumulating in the BM of sham-operated or Sp_x naïve (open bars) and infected (black bars) mice. Data from one experiment (n=5 mice per group; Mann-Whitney: not significant (ns). **B.** T cell accumulation in BM visualized using hCD2-DsRed mice. Sectioned were counterstained with DAPI (blue). Femurs representative of 15 mice per group examined from 3 independent experiments. **C and D.** Absolute numbers of pro-erythroblasts (C) and erythroblasts (D) in the BM of naïve and infected wild type C57BL/6 or B6.*Rag2*$^{-/-}$ mice. Absolute numbers were calculated by multiplying frequencies by the total BM cell counts (One-way ANOVA with Turkey's multiple comparison test; n=10 mice per group from 2 independent experiments). Data represent mean ± SEM. **E.** *Cxcl12* mRNA accumulation in total BM cells from naïve and infected B6.*Rag2*$^{-/-}$ mice. Intra-sample standardization was performed by normalization to HPRT and inter-sample standardization was done by normalization to the average expression of the naïve group (n=8 wild-type mice per group, 5 naïve and 7 infected from one experiment). **F.** CD169 expression on BM macrophages of naïve (green) and infected (red) B6.*Rag2*$^{-/-}$ mice. Isotype control (blue) is representative of both naïve and infected mice. **G.** Absolute numbers of macrophages per leg (1 femur + 1 tibia), calculated from the frequencies multiplied by the total bone marrow cells isolated from each mouse (n=3 naïve and 4 infected mice from one experiment). **H and I.** Anemia, measured as RBC count (H) or hematocrit (I) in B6.*Rag2*$^{-/-}$ mice receiving adoptive transfer of either IFNγ-sufficient (WT) or IFNγ-deficient (IFNγKO) CD4$^+$ T cells**.** **(**n=4/5 per group; One-way Anova followed by Tukey's multiple comparisons test: not significant (ns), *$p \leq 0.05$).

686 **Table 1. Hematological characteristics of C57BL/6 mice infected for 28 days with *L.***

687 ***donovani.***

	Naive	***Infected***
WBC (x10^3/ul)	6.803 ± 0.864	5.758 ± 0.659
NE (x10^3/ul)	1.671 ± 0.309	1.108 ± 0.128
LY (x10^3/ul)	4.486 ± 0.455	4.072 ± 0.626
MO (x10^3/ul)	0.296 ± 0.072	0.230 ± 0.017
EO (x10^3/ul)	0.259 ± 0.077	0.108 ± 0.058
BA (x10^3/ul)	0.077 ± 0.026	0.013 ± 0.003
RBC (x10^6/ul)	8.110 ± 0.143	**6.572 ± 0.241*** **
HB (g/dl)	9.593 ± 0.213	**8.169 ± 0.219*** **
HCT (%)	41.860 ± 0.900	**34.020 ± 1.091*** **
MCV (fl)	51.610 ± 0.577	51.990 ± 1.035
MCH (pg)	11.860 ± 0.227	**12.520 ± 0.198***
MCHC (g/dl)	23.040 ± 0.663	24.130 ± 0.509
PLT (x10^3/ul)	583.000 ± 45.680	**281.500 ± 26.39*** **
MPV (fl)	4.293 ± 0.143	**5.354 ± 0.084*** **

688

689 Bold values are significant: *p<0.05; *** p<0.0001

690

691 **Table 2. Comparative myelogram of naïve mice and mice infected with *L. donovani* for**

692 **28 days.**

693

	Naive	***Infected***
Myeloid : Erythoid Ratio	1.5 (1.3-2.0)	**2.1 (1.7-2.8)***
Precursor Myeloid : Mature Myeloid	0.02 (0.01-0.03)	**0.1 (0.04-0.19)***
Nucleated Erythroid Precursor : Nucleated Erythroid Mature	0.02 (0.01-0.03)	0.03 (0.02-0.05)
Precursor Myeloid Cells (%)	1.0 (0.6-1.1)	**4.8 (2.6-6.0)***
Mature Myeloid Cells (%)	39.7 (35.5-42.5)	**34.8 (31.0-38.1)***
Nucleated Erythroid Precursor Cells (%)	0.6 (0.4-0.9)	0.6 (0.2-0.9)
Nucleated Erythroid Mature Cells (%)	26.8 (19.4-30.6)	**17.8 (11.8-21.1)***
Lymphocytes (%)	33.0 (26.4-37.4)	**41.2 (35.7-47.2)***
Plasma cells (%)	0.4 (0.2-0.6)	0.6 (0.2-1.0)
Monocytes (%)	0.0 (0.0-0.2)	0.3 (0.0-0.7)
Macrophages (%)	0.0 (0.0-0.2)	0.0 (0.0-0.1)

694

695 Bold values are significant: *$p<0.05$

Supporting Information Legends

S1 Table. Distribution of infected mice according to normal values of haematological parameters.

S1 Figure Aberrant red cell morphology following *L. donovani* infection

Representative images of M-G Giemsa-stained blood films from naïve (A-D) and d28 *L. donovani*-infected mice (E-H). Red thin arrow: polychromatic red cells; green thin arrow: acanthocytes; yellow thin arrow: schistocytes; black thin arrow: macrocyte; white thin arrow: microcyte; blue thin arrow: elliptocyte; red large arrow: nucleated red blood cell; blue large arrow: lymphocyte; green large arrow: neutrophil.

S2 Figure. Frequency of erythroid precursors in bone marrow.

Frequency of erythroid precursors (pro-erythroblasts and erythroblasts) in the bone marrow of naïve (green) and *L. donovani*-infected (red) B6 mice over time. Precursors were identified on the basis of TER119 and CD71 staining. Unpaired t-test; n=3 mice per group per timepoint).

S3 Figure Myelogram of *L. donovani*-infected BM

BM samples were obtained by aspiration biopsy from iliac crest using 24 G needle attached to a 5mL disposable plastic syringe with 10% EDTA and smears were stained with May–Grünwald Giemsa and analyzed by optical microscopy (Zeiss, Germany) and images using Zen software (Carl Zeiss). A Binucleated erythroid cell. B Megalocyte. C. Atypical mitosis. D Emperipolesis. Examples of such cells are indicated with arrows.

S4 Figure Frequency of T cells in bone marrow

Frequency of $CD3^+$ cells in the bone marrow of naïve (green) and *L. donovani*-infected (red) B6 mice over time. Unpaired t-test; n=3 mice per group per timepoint).

S5 Figure. Parasite load in *L. donovani* infected B6 and B6.*Rag2*$^{-/-}$ mice.

Parasites per 1000 nuclei in the spleen at d28 p.i.. Spleen impressions smears were made on glass slides and stained with Giemsa. Parasites and nuclei were counted microscopically. n=8 wild-type and 6 $RAG2^{-/-}$ mice from 2 independent experiments

S6 Figure. Number and differentiation state of wild type and IFNγ KO $CD4^+$ T cells in RAG recipients.

Wild type (black bars) or IFNγ KO (open bars) $CD4^+$ T cells were transferred into RAG recipients prior to infection with *L. donovani*. At day 28 p.i., BM $CD4^+$ T cells were enumerated and characterized by flow cytometry. **A.** Number of total $CD4^+$ T cells and of $CD4^+$ T cells with $CD44^{hi}$ and $CD44^{lo}$ phenotype. **B.** Number of $CD4^+$ T cells expressing different expression patterns for Ly6C, CD44 and CD127. $CD44^{hi}Ly6C^{-/lo}CD127^{-/lo}$ are often regarded as classical effector cells. Two tibias and femurs were taken per mouse with n=4 mice receiving wild type T cells and n=5 mice receiving KO T cells.

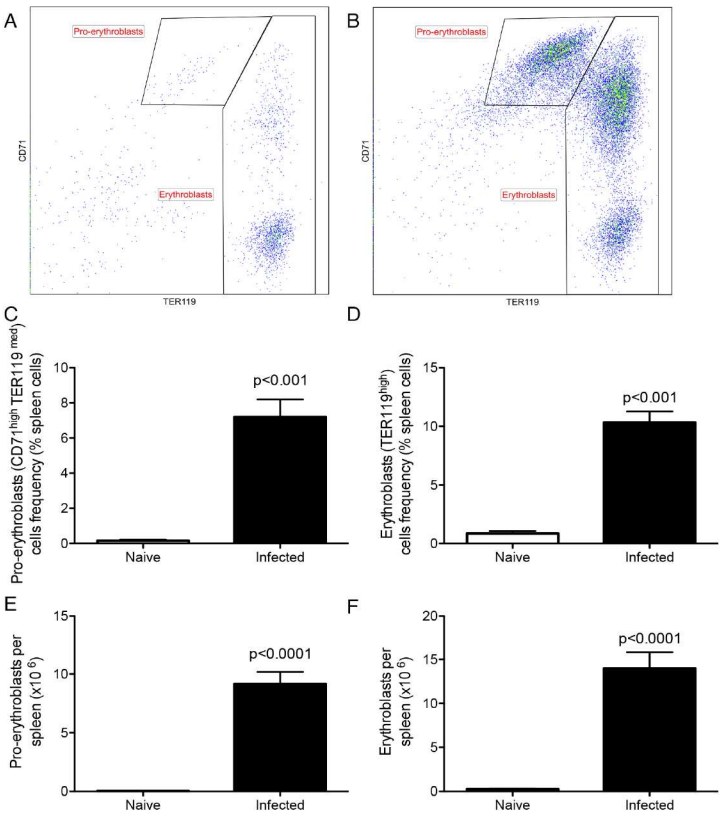
A
Pro-erythroblasts
Erythroblasts
CD71
TER119
B
Pro-erythroblasts
Erythroblasts
CD71
TER119
C
Pro-erythroblasts (CD71high TER119 med) cells frequency (% spleen cells)
p<0.001
Naive
Infected
D
Erythroblasts (TER119high) cells frequency (% spleen cells)
p<0.001
Naive
Infected
E
Pro-erythroblasts per spleen (x10 6)
p<0.0001
Naive
Infected
F
Erythroblasts per spleen (x10 6)
p<0.0001
Naive
Infected

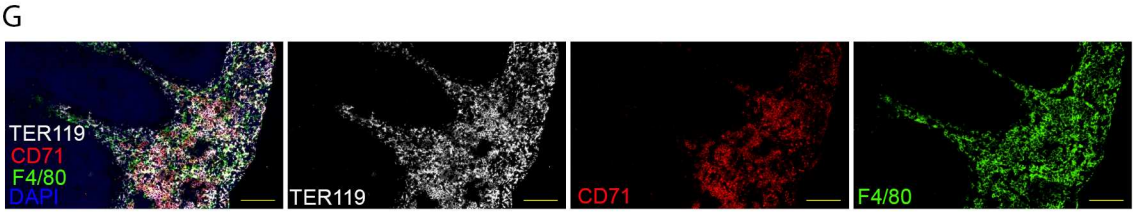
G
TER119
CD71
F4/80
DAPI
TER119
CD71
F4/80

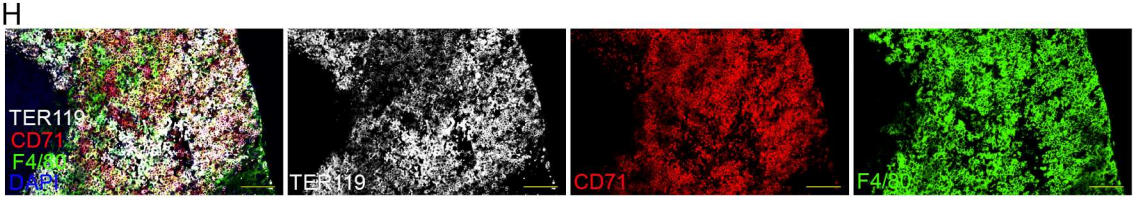
H
TER119
CD71
TER119
CD71

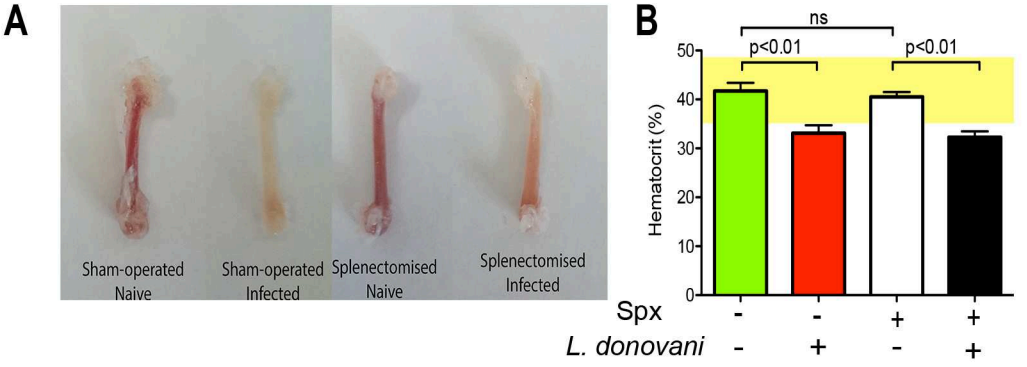
A
Sham-operated Naive
Sham-operated Infected
Splenectomised Naive
Splenectomised Infected
B
ns
p<0.01
p<0.01
Hematocrit (%)
50
40
30
20
10
0
Spx - - + +
L. donovani - + - +
C
Naive
50 µm
D
28d p.i.
TER119
DAPI
E
Pro-erythroblasts
Erythroblasts
CD71
TER119
F
ns
p<0.001
p<0.001
Erythroblasts per femur + tibia (x10 6)
3
2
1
0
Spx - - + +
L. donovani - + - +

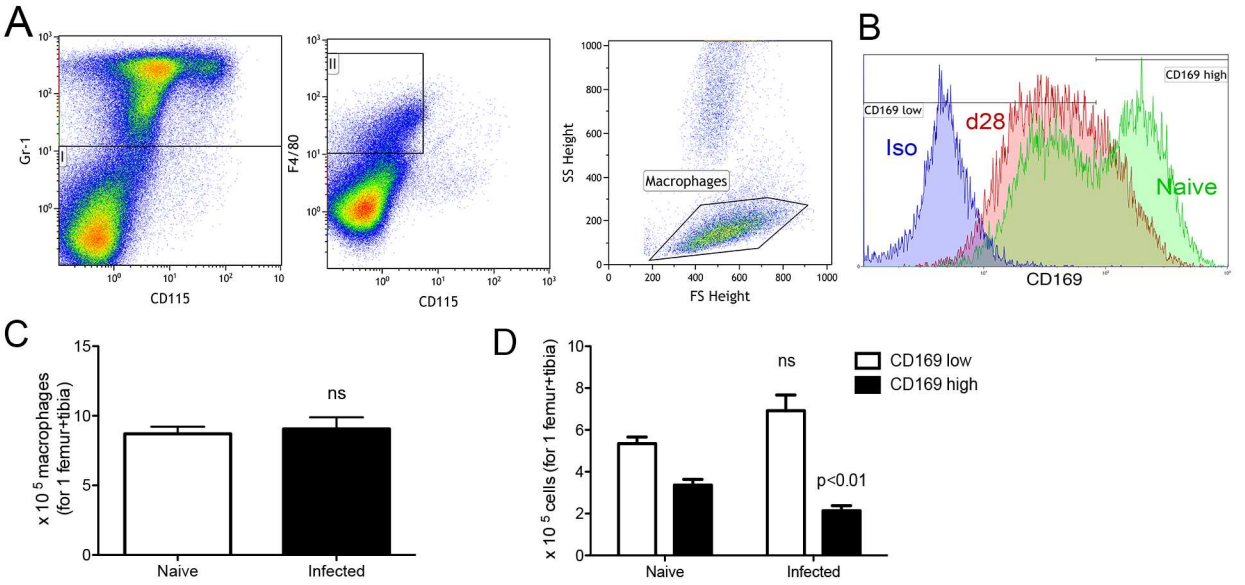
A
Gr-1
CD115
I
F4/80
CD115
II
SS Height
FS Height
Macrophages
B
CD169 low
CD169 high
Iso
d28
Naive
CD169
C
x 10 5 macrophages (for 1 femur+tibia)
ns
Naive
Infected
D
x 10 5 cells (for 1 femur+tibia)
ns
p<0.01
CD169 low
CD169 high
Naive
Infected

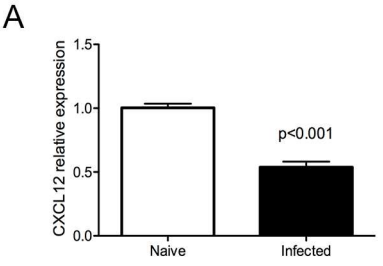
A
CXCL12 relative expression
1.5
1.0
0.5
0.0
p<0.001
Naive
Infected

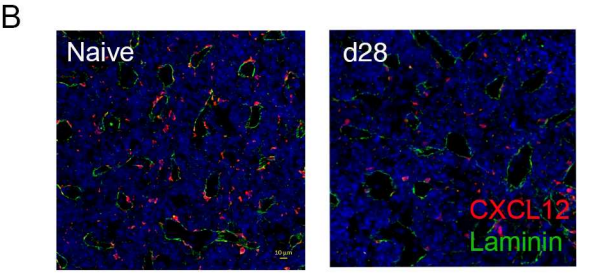
B
Naive
d28
CXCL12
Laminin

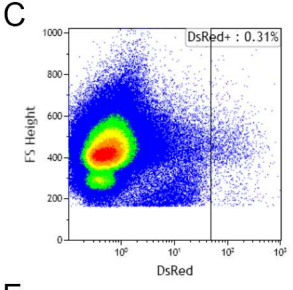
C
DsRed+ : 0.31%
FS Height
DsRed

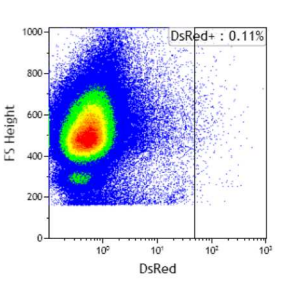
D
DsRed+ : 0.11%
FS Height
DsRed

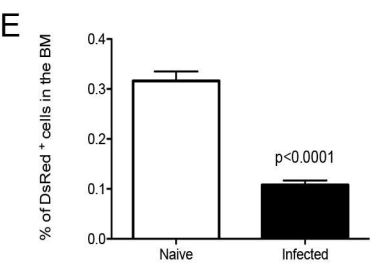
E
% of DsRed + cells in the BM
0.4
0.3
0.2
0.1
0.0
p<0.0001
Naive
Infected

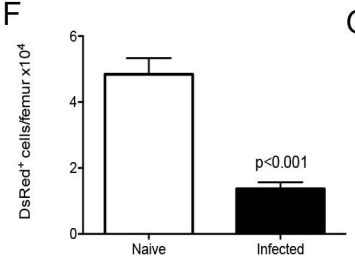
F
DsRed+ cells/femur x10^4
6
4
2
0
p<0.001
Naive
Infected

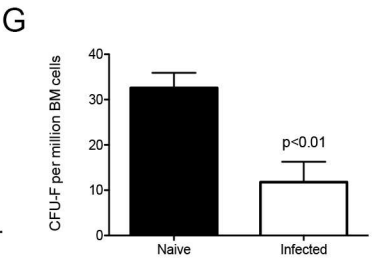
G
CFU-F per million BM cells
40
30
20
10
0
p<0.01
Naive
Infected

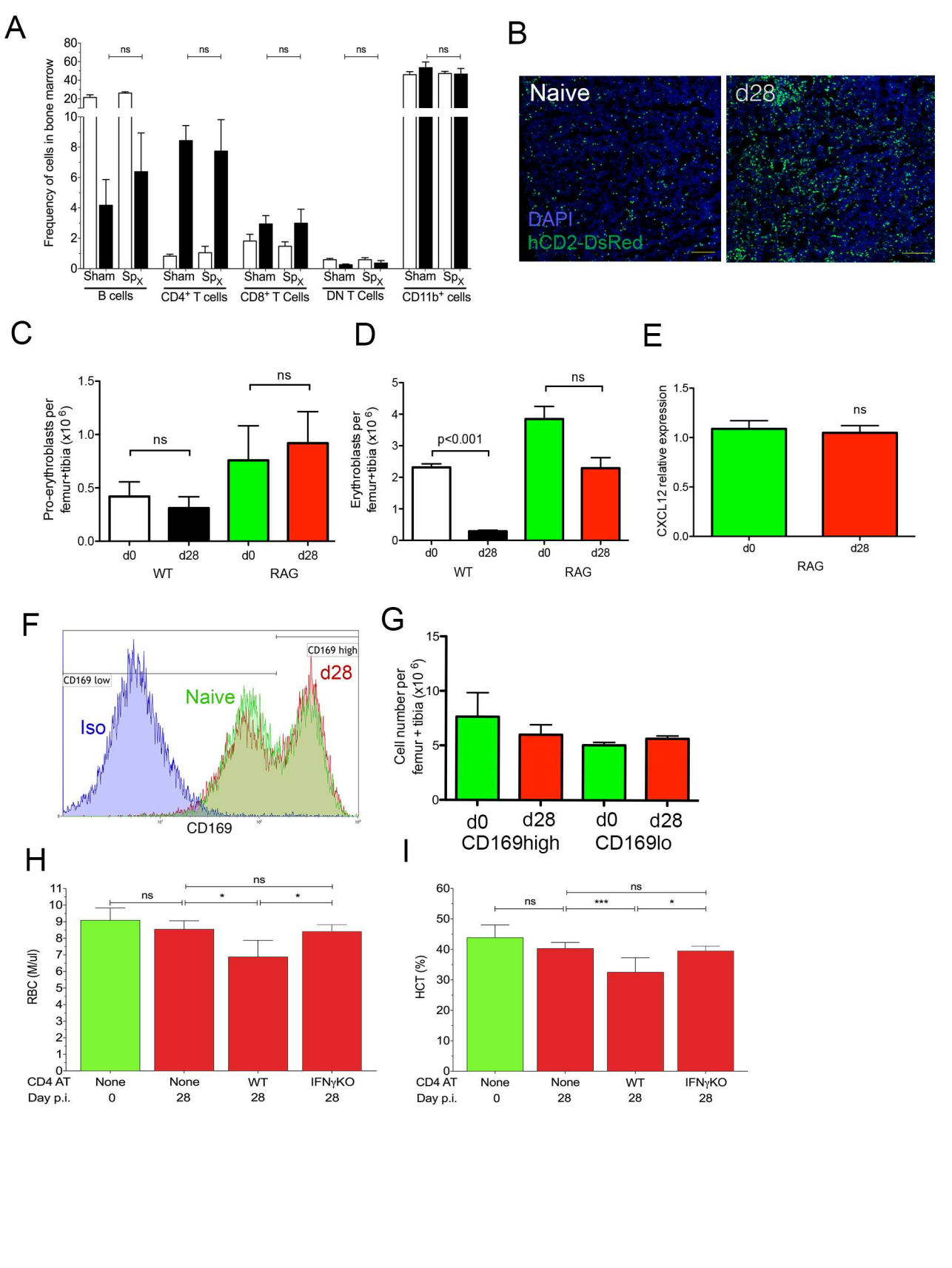
A
Frequency of cells in bone marrow
ns
Sham
SpX
B cells
CD4+ T cells
CD8+ T Cells
DN T Cells
CD11b+ cells
B
Naive
d28
DAPI
hCD2-DsRed
C
Pro-erythroblasts per femur+tibia (x10 6)
p<0.001
d0
d28
WT
RAG
D
Erythroblasts per femur+tibia (x10 6)
E
CXCL12 relative expression
F
CD169 low
CD169 high
Iso
Naive
d28
CD169
G
Cell number per femur + tibia (x10 6)
d0 CD169high
d28 CD169high
d0 CD169lo
d28 CD169lo
H
RBC (M/ul)
CD4 AT
Day p.i.
None
WT
IFNγKO
I
HCT (%)

CD4^{+} T cells alter the stromal microenvironment and repress medullary erythropoiesis in murine visceral leishmaniasis. Preham et. al.

S1 Table. Distribution of infected mice according to normal values of haematological parameters.

	Reference interval	*Distribution relative to reference interval (%)*		
		Under	**Within**	**Above**
WBC (x10^3/ul)	2.40 - 15.73	0	100	0
NE (x10^3/ul)	0.37 - 5.03	0	100	0
LY (x10^3/ul)	1.96 - 9.01	7.69	92.31	0
MO (x10^3/ul)	0.05 - 0.92	0	100	0
EO (x10^3/ul)	0.01 - 0.71	0	92.31	7.69
BA (x10^3/ul)	0.00 - 0.26	0	100	0
RBC (x10^6/ul)	7.04 - 9.18	69.23	30.77	0
HB (g/dl)	8.00 - 11.19	30.77	69.23	0
HCT (%)	35.12 - 48.60	61.54	38.46	0
MCV (fl)	47.30 - 55.92	0	76.92	23.08
MCH (pg)	10.16 - 13.56	0	100	0
MCHC (g/dl)	18.08 - 28.00	0	100	0
PLT (x10^3/ul)	241.20 - 924.80	38.46	61.54	0
MPV (fl)	3.60 - 5.00	0	23.08	76.92

Supplementary Figures

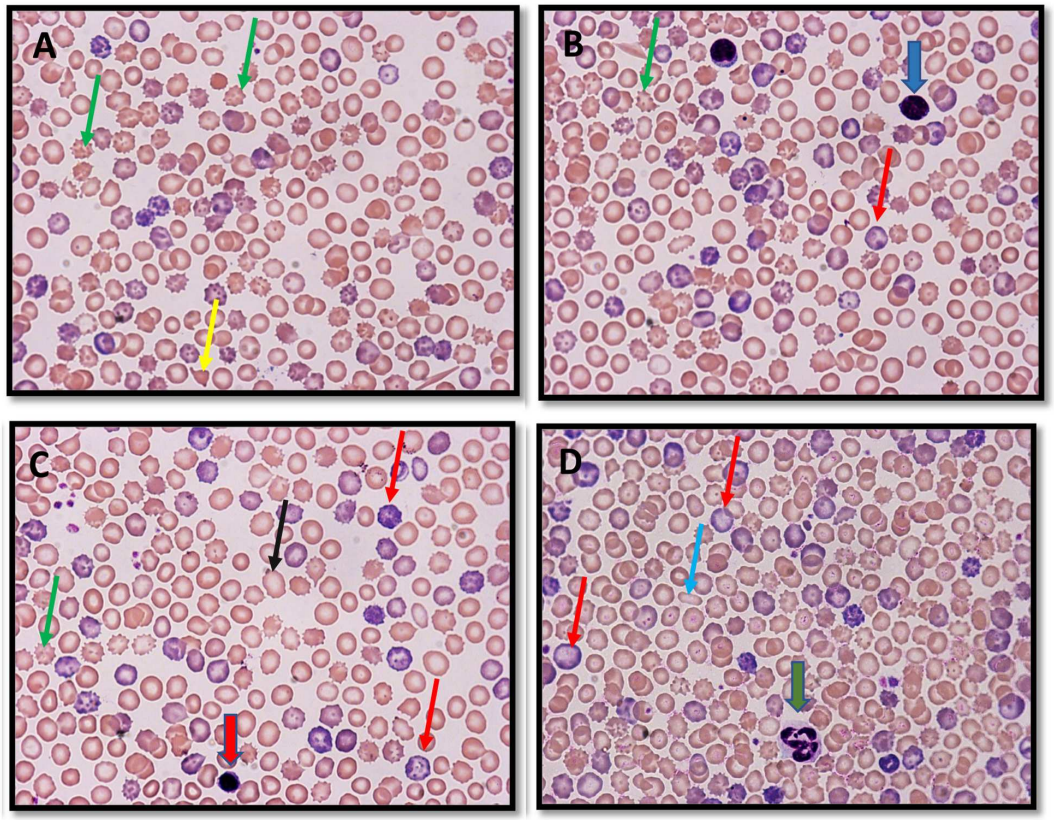

S1 Figure Aberrant red cell morphology following *L. donovani* infection

Representative images of M-G Giemsa-stained blood films from d28 *L. donovani*-infected mice. **A.** green thin arrow: acanthocytes; yellow thin arrow: schistocytes; **B.** red thin arrow: polychromatic red cells; blue large arrow: lymphocyte; **C.** red large arrow: nucleated red blood cell; black thin arrow: macrocyte; **D.** green large arrow: neutrophil. blue thin arrow: elliptocyte

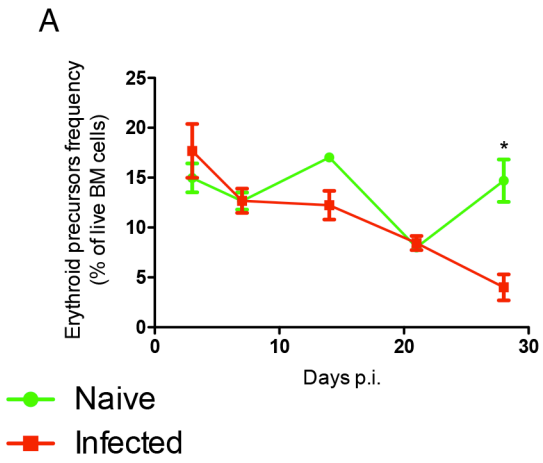

S2 Figure. Frequency of erythroid precursors in bone marrow.

Frequency of erythroid precursors (pro-erythroblasts and erythroblasts) in the bone marrow of naïve (green) and *L. donovani*-infected (red) B6 mice over time. Precursors were identified on the basis of TER119 and CD71 staining. Unpaired t-test; n=3 mice per group per timepoint).

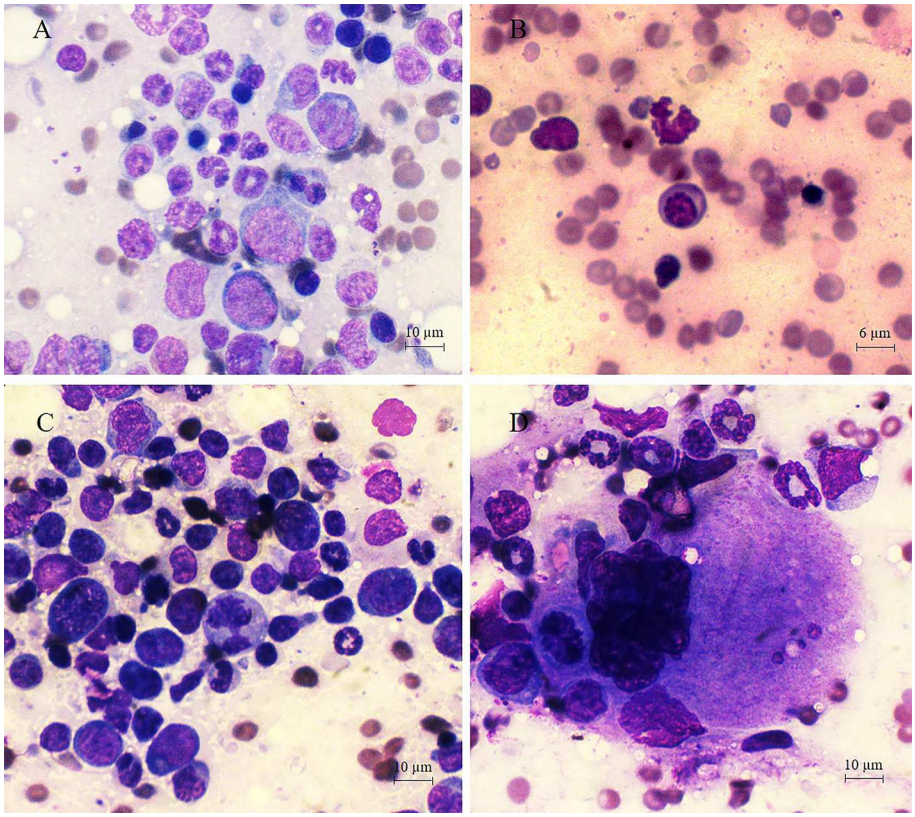

S3 Figure Myelogram of *L. donovani*-infected BM

BM samples were obtained by aspiration biopsy from iliac crest using 24 G needle attached to a 5mL disposable plastic syringe with 10% EDTA and smears were stained with May–Grünwald Giemsa and analyzed by optical microscopy (Zeiss, Germany) and images using Zen software (Carl Zeiss). A Binucleated erythroid cell. B Megalocyte. C. Atypical mitosis. D Emperipolesis.

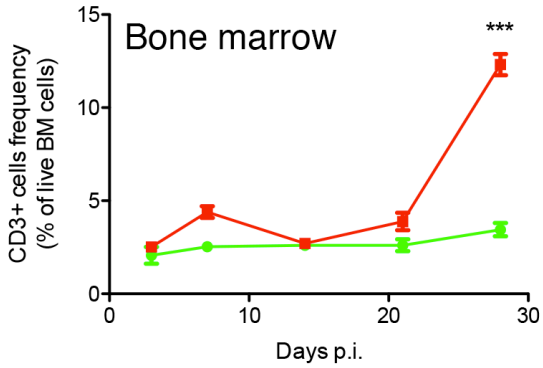

S4 Figure Frequency of T cells in bone marrow

Frequency of $CD3^+$ cells in the bone marrow of naïve (green) and *L. donovani*-infected (red) B6 mice over time. Unpaired t-test; n=3 mice per group per timepoint).

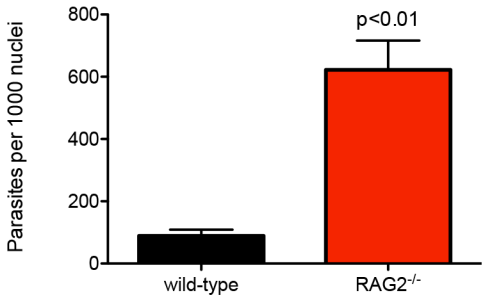

S5 Figure. Parasite load in *L. donovani* infected B6 and B6.*Rag2*$^{-/-}$ mice.

Parasites per 1000 nuclei in the spleen at d28 p.i.. Spleen impressions smears were made on glass slides and stained with Giemsa. Parasites and nuclei were counted microscopically. n=8 wild-type and 6 RAG2$^{-/-}$ mice from 2 independent experiments.

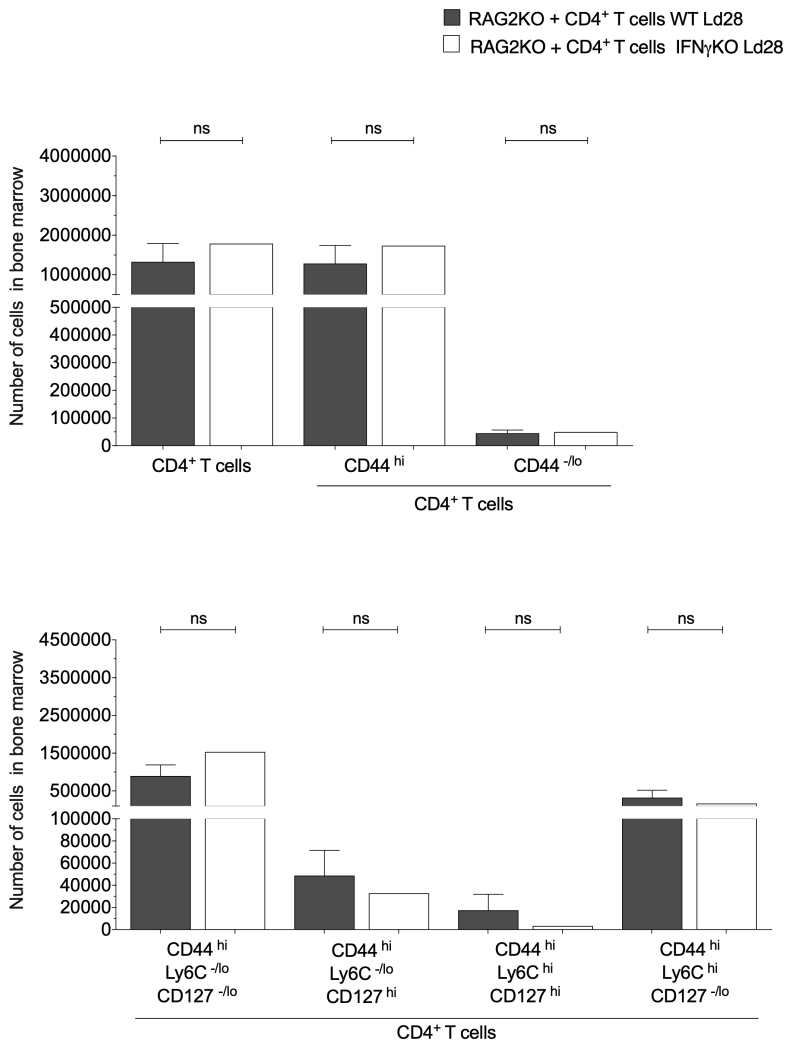

S6 Figure. Number and differentiation state of wild type and IFNγ KO CD4$^+$ T cells in RAG recipients.

Wild type (black bars) or IFNγ KO (open bars) CD4$^+$ T cells were transferred into RAG recipients prior to infection with *L. donovani*. At day 28 p.i., BM CD4$^+$ T cells were enumerated and characterized by flow cytometry. **A.** Number of total CD4$^+$ T cells and of CD4$^+$ T cells with CD44^{hi} and CD44^{lo} phenotype. **B.** Number of CD4$^+$ T cells expressing different expression patterns for Ly6C, CD44 and CD127. CD44^{hi}Ly6C$^{-/lo}$CD127$^{-/lo}$ are often regarded as classical effector cells. Two tibias and femurs were taken per mouse with n=4 mice receiving wild type T cells and n=5 mice receiving KO T cells.